



## Downscaling Landsat 7 canopy reflectance employing a multi-soil sensor platform

Elia Scudiero<sup>1</sup> · Dennis L. Corwin<sup>1</sup> · Brian J. Wienhold<sup>2</sup> · Bruce Bosley<sup>3</sup> · John F. Shanahan<sup>4</sup> · Cinthia K. Johnson<sup>5</sup>

© Springer Science+Business Media New York (outside the USA) 2015

**Abstract** Crop growth and yield can be efficiently monitored using canopy reflectance. However, the spatial resolution of freely available remote sensing data is too coarse to fully understand the spatial dynamics of crop status. The objective of this study was to downscale Landsat 7 (L7) reflectance from the native resolution of  $30 \times 30$  m to that typical of yield maps (ca.  $5 \times 5$  m) over two fields in northeastern Colorado, USA. The fields were cultivated with winter wheat (*Triticum aestivum* L.) in the 2002–2003 growing season. Geospatial yield measurements were available (1 per ca.  $20 \text{ m}^2$ ). Geophysical (apparent soil electrical conductivity and bare-soil imagery) and terrain (micro-elevation) data were acquired (resolution  $<5 \times 5$  m) to characterize soil spatial variability. Geographically-weighted regressions were established to study the relationships between L7 reflectance and the geophysical and terrain data at the  $30 \times 30$  m scale. Geophysical and terrain sensors could describe a large portion of the L7 reflectance spatial variability ( $0.83 < R^2 < 0.94$ ). Maps for regression parameters and intercept were obtained at  $30 \times 30$  m and used to estimate the L7 reflectance at  $5 \times 5$  m resolution. To independently assess the quality of the downscaling procedure, yield maps were used. In both fields, the  $5 \times 5$  m estimated reflectance showed stronger correlations (average increase in explained variance = 3.2 %) with yield than at the  $30 \times 30$  m resolution. Land resource managers, producers, agriculture consultants, extension specialists and Natural Resource Conservation Service field staff would be the beneficiaries of downscaled L7 reflectance data.

---

✉ Elia Scudiero  
elia.scudiero@ars.usda.gov; scudiero@dmsa.unipd.it

<sup>1</sup> United States Salinity Laboratory, USDA-ARS, 450 West Big Springs Rd., Riverside, CA 92507-4617, USA

<sup>2</sup> Agroecosystem Management Research Unit, USDA-ARS, Keim Hall University of Nebraska-Lincoln-East Campus, Lincoln, NE 68583, USA

<sup>3</sup> Colorado State University Extension, 508 South 10th Ave., Sterling, CO 80751, USA

<sup>4</sup> DuPont Pioneer Hi-Bred International Inc., 6807 Ridge Rd., Lincoln, NE 68512, USA

<sup>5</sup> Plainview Farms, Inc., 11416 County Road 63, Sterling, CO 80751, USA

**Keywords** Landsat 7 · Downscaling · Apparent electrical conductivity · Bare-soil imagery · Micro-elevation · Geographically-weighted regression

### Abbreviations

L7	Landsat 7
EC <sub>a</sub>	Apparent electrical conductivity
BS	Bare-soil
GWR	Geographically-weighted regression

## Introduction

The delineation of crop input prescription maps in precision agriculture (e.g., maps of site-specific management units for fertilizer, irrigation water, soil amendments, etc.) relies on a careful study of the spatial variability of soil–plant relationships. Yield maps provide pivotal information to implement precision agriculture techniques. However, they are often characterized by noise in the data due to yield monitor and combine grain flow dynamics and only provide a single “snapshot” in time (i.e., at the time of harvest) (Blackmore 1999; Corwin et al. 2003; Ping and Dobermann 2005). To better understand soil–plant relationships through the growing season, crop canopy reflectance can be used (Mulla 2013). Remote sensing canopy reflectance is used to predict production (Shanahan et al. 2001) and estimate crop stress status through the season (Blackmer et al. 1995; Vina et al. 2004). One clear benefit of the use of remote sensing over yield maps is the possibility of studying spatio-temporal changes in crop development through the growing season. This dynamic information can substantially help in understanding soil–plant relationships and soil-related stress types, such as drought (Scudiero et al. et al. 2014b).

The new generation of satellites, such as Spot 5 and Spot 6 (Airbus Defence & Space, Toulouse, France) and Quickbird and WorldView 2 and 3 (DigitalGlobe, Longmont, Colorado, USA), provide multi-spectral data in the visible to infrared spectra that can be extremely useful in precision agriculture because of their high spatial resolution (in the 4–100 m<sup>2</sup> range) and low repeat interval (e.g., 1.1 days for WorldView-2) (Mulla 2013). However, because of the greater expense associated with acquiring high resolution satellite imagery, extensive use of these data sources in precision agriculture at the farm-scale (e.g., 10<sup>2</sup>–10<sup>3</sup> ha) has been limited. Instead, lower resolution satellite data is often used. A popular source of free satellite sensor data provided at a moderately high resolution is the Landsat 7 (L7) from the National Aeronautics and Space Administration and Geological Survey (USGS) USA agencies. The L7 provides reflectance imagery with a 30 × 30 m resolution over six spectral bands (see materials and methods). The L7 flies over the same area every 16 days, potentially providing significant information for spatio-temporal studies of crop health (Scudiero et al. 2014b). Unfortunately, as suggested by Scudiero et al. (2014a), the 30 × 30 m resolution is generally too coarse to fully capture crop and soil spatial variability, a clear downside for the use of L7 data in precision agriculture practices.

Soil spatial variability is often described using soil proxy data (e.g., geophysical sensors and/or terrain maps), which can characterize large areas while requiring calibration with only a small number of soil samples (Adamchuk et al. 2004; Corwin and Lesch 2010; Priori et al. 2013a). Unfortunately, a single sensor might not always be sufficient to

describe the spatial distribution of all the soil properties influencing yield (Scudiero et al. 2013). Sensor measurements are, in fact, generally dominated by one or two soil properties (Corwin and Lesch 2014). In order to obtain additional information on soil spatial variability, multi-sensory platforms are used (Martini et al. 2013, Priori et al. 2013b; Schepers et al. 2004).

The most common type of spatial geophysical measurement used to characterize soil spatial variability is soil apparent electrical conductivity ( $EC_a$ ) (Corwin and Lesch 2010). Depending on the geographical region,  $EC_a$  can be a proxy for a number of soil properties (Corwin and Lesch 2010), as soil electrical conductivity is influenced by many factors including soil salinity, texture, water content, bulk density and organic matter content. In addition to  $EC_a$ , bare-soil imagery/reflectance is commonly used as a proxy to map soil properties including water content, texture, carbon content, iron oxides, organic matter and high levels of soil salinity (Chang et al. 2001; Ellis and Mellor 2002; Viscarra Rossel et al. 2006). In addition to geophysical measurements, which are physically determined by soil properties, terrain information, such as micro-elevation, could be used to describe spatial variability (Iqbal et al. 2005; Kravchenko et al. 2002; Schmidt and Persson 2003) of soil properties (locally) as influenced by the geomorphological characteristics of the area of interest. Terrain features such as micro-elevation, slope and aspect maps have been used successfully to describe spatial variability in soil moisture and changes in soil texture and organic carbon caused by erosion processes (Iqbal et al. 2005; Kravchenko and Robertson 2007; Schmidt and Persson 2003).

The goal of this study was to provide land resource managers, producers, agricultural advisors and extension specialists with an inexpensive option for the use of high resolution canopy reflectance. In particular, a downscaling procedure that allows sharpening the L7 data from a spatial resolution of  $30 \times 30$  m to that typical of yield maps (e.g.,  $5 \times 5$  m, or higher) is proposed. The downscaling methodology is based on the notions that: (i) remote sensing crop reflectance indicates crop health, unless the noise from other factors influencing both yield and surface reflectance (e.g., weeds, see Braga et al. 2012) is too large (Lobell et al. 2003), and (ii) crop growth is greatly influenced by edaphic properties (Corwin et al. 2003; Savabi et al. 2013).

## Materials and methods

Once soil properties are spatially characterized and their relationship with plant health is known, one can easily and accurately describe the spatial variability of crop yield/health. Very-high resolution maps of soil proxies will be used to characterize the spatial variations in L7 canopy reflectance and, consequently, downscale it. The presented methodology follows a multi-step approach for selecting the ideal multi (soil-) sensor platform:

- Acquire intense geospatial survey with available soil sensors. Sensor data acquisition should be carried out according to shared protocols (e.g., Corwin and Lesch 2005) in order to increase the accuracy and consistency of the survey across large areas;
- Carry out root-zone soil physical and chemical analysis over limited locations in the study area. Sampling site number can be minimized using statistical modeling (Lesch 2005a; Van Groenigen and Stein 1998) according to the spatial variability of soil properties (e.g., represented by soil sensors);
- Measure yield across each location and analyze soil-plant (yield/health) relationships (e.g., Corwin et al. 2003; Scudiero et al. 2013);

- Using the available set of sensor data, select those sensors which represent the spatial variability of soil properties influencing crop yield/health (Priori et al. 2013b; Scudiero et al. 2013).

Once a good soil multi-sensor platform is selected, the sensor data can be used to describe crop health/yield spatial variability and consequently to drive the spatial down-scaling of the L7 canopy reflectance from native reflectance to that of the soil sensors (usually higher than  $2 \times 2$  m).

To independently assess the quality of this procedure, the relationships between observed yield data and reflectance at  $30 \times 30$  m and sharpened ( $5 \times 5$  m) scales will be discussed.

## The study area

Two study fields cropped with winter wheat (*Triticum aestivum* L.) were investigated (Fig. 1). The fields are about 30 km east of Sterling, in northeastern Colorado, in the semi-arid Central Great Plains of the USA. The two fields were described in previous publications (Johnson et al. 2003a, b, 2008). Consistent with these studies, the two fields were named F5 and F8 (Fig. 1). F5 is 23.9 ha, whereas F8 is 32.8 ha. Soils are a mixture of Platner (fine, smectitic, mesic Aridic Paleustolls), Weld (fine, smectitic, mesic Aridic Argiustolls), and Rago (fine, smectitic, mesic Pachic Argiustolls) loams (USDA *Soil Taxonomy*). The regional climate is cool and semi-arid with a mean annual temperature of  $10^\circ\text{C}$  and mean annual rainfall of 420 mm. Precipitation is highly variable, with 75 % falling between April and September, mostly concentrated in May, June and July. The data discussed in this manuscript refers to the cropping season of 2002–2003, when winter wheat was sowed in mid-September 2002 and harvested in early July 2003, and the fields were under no-tillage management. The fields in this study were (and continue to be) farmed in a winter wheat, maize (*Zea mays* L.), proso millet (*Panicum miliaceum* L.) and fallow rotation. Note that the wheat phase of the rotation follows a fallow year where no



**Fig. 1** Map of the two study sites (F5 and F8), located in northeast Colorado, USA. The soil sampling locations are shown (Color figure online)

crop is grown and weeds are controlled. This is done in an effort to store water for the following year's wheat crop even though fallow stores, at best, only 40 % of the available precipitation. Precipitation for the actual wheat cropping season (9/2002–7/2003) was 287 mm—far short of average (precipitation occurs mainly in May and June, averaging 420 mm annually). To make matters worse, precipitation during the entire fallow year (9/2001–9/2002) was a mere 157 mm. This data comes from the National Weather Service which, at the time, had its collection site ca. 1.5 km west of the fields addressed in this study.

### **Landsat 7 canopy reflectance**

The Landsat 7 (L7) satellite sensor provides reflectance imagery with a  $30 \times 30$  m resolution over six spectral bands, namely: blue (B, 450–520 nm), green (G, 520–600 nm), red (R, 630–690 nm), near-infrared (NIR, 770–900 nm), shortwave infrared 1 (IR1, 1550–1750 nm) and shortwave infrared 2 (IR2, 2090–2350 nm). Atmospherically-corrected L7 reflectance data is freely provided by US Geological Survey (<http://earthexplorer.usgs.gov/>) as Landsat 7 climate data record (CDR) surface reflectance. The L7 CDR imagery is atmospherically corrected through the Landsat Ecosystem Disturbance Adaptive Processing System according to Masek et al. (2006).

Eleven cloudless L7 scenes were available over the two fields, through the wheat growing season (September 28, October 14, November 15, December 1 and 17 in 2002; and January 1, February 20, March 8, April 9 and May 11 and 30 in 2003). For brevity, this manuscript will present the spatial downscale of the seasonal average reflectance for each L7 spectral band.

### **Geophysical and terrain data**

The ancillary data considered in this study were: soil apparent electrical conductivity (geophysical), aerial bare-soil reflectance intensity (geophysical) and micro-elevation (terrain).

In April 2005, the fields were surveyed with intensive electromagnetic induction (EMI) measurements, using an EM38 (Geonics Ltd., Mississauga, Ontario, Canada) Dual Dipole sensor connected to a DGPS and mounted on a non-metallic sled, following the protocols given by Corwin and Lesch (2005). The EM38 measured soil apparent electrical conductivity ( $EC_a$ ) at 11583 and 15731 locations in F5 and F8, respectively, for both the 0–0.75 and 0–1.50 m soil profiles obtained from EMI measurements of  $EC_a$  taken in the horizontal ( $EC_aH$ ) and vertical ( $EC_aV$ ) configurations, respectively. The EM38 readings are characterized by a spatial resolution of about 1–2 m<sup>2</sup>.  $EC_a$  acquisitions were made every ~6.5 m along the same transect. Swath distance between transects was about 10–12 m.

Bare-soil aerial imagery over F5 and F8 was downloaded from the US Geological Survey Earth Explorer database (<http://earthexplorer.usgs.gov/>). The aerial orthophoto was acquired on the 14th of July 2011 by the National Agriculture Imagery Program (NAIP) with the ADS40 (Leica Geosystem, Heerbrugg, Switzerland) digital sensor. The four-band imagery (blue at 430–490 nm, green at 535–585 nm, red at 610–660 nm and near-infrared at 835–885 nm) have a discrete value ranging from 0 to 255, based on the original bare-soil reflectance intensity. The NAIP orthophoto has spatial resolution of  $1 \times 1$  m.

Micro-elevation at the field was assessed in April 2005 at 1945 and 2002 locations over F5 and F8, respectively, with a Radian IS and GRS 2600 (Sokkia Inc., Kansas, USA) Real

**Table 1** Winter wheat yield, apparent electrical conductivity for the 0–0.75 m ( $EC_aH$ ) and 0–1.5 m ( $EC_aV$ ) soil profiles, and micro-elevation data summary: mean and range statistics, exponential isotropic semi-variogram specifications, and cross validation root mean square errors (RMSE) over the two block supports (25 and 900 m<sup>2</sup>)

Field	Variable	Average		Maximum	SD	Exponential isotropic semi-variogram specifications				Kriging (block support) cross-validation RMSE	
		Minimum	Maximum			Nugget	Partial Sill	Lag (m)	Range (m)	5 × 5 m	30 × 30 m
5	Yield (Mg ha <sup>-1</sup> )	2.3	0.1	6.5	0.57	0.2	0.7	5.0	60.0	0.26	0.48
	$EC_aH$ (dS m <sup>-1</sup> )	0.19	0.08	0.29	0.03	0.2	0.8	11.0	95.2	0.01	0.02
	$EC_aV$ (dS m <sup>-1</sup> )	0.28	0.14	0.45	0.05	0.0	1.0	11.0	120.8	0.01	0.02
	Elevation (m)	1354.1	1351.7	1356.8	1.2	0.0	1.4	17.5	210.0	0.02	0.14
8	Yield (Mg ha <sup>-1</sup> )	2.6	0.1	6.3	0.77	0.0	0.8	5.0	39.9	0.15	0.47
	$EC_aH$ (dS m <sup>-1</sup> )	0.22	0.12	0.34	0.03	0.0	1.0	8.0	79.1	0.01	0.02
	$EC_aV$ (dS m <sup>-1</sup> )	0.23	0.11	0.37	0.04	0.0	1.0	8.0	96.0	0.01	0.02
	Elevation (m)	1350.3	1347.7	1353.2	1.2	0.1	1.0	12.3	120.8	0.05	0.12

Time Kinematic system. In F5, elevation ranged between 1351.7 and 1356.8 m above sea level (asl), whereas in F8 it ranged between 1347.7 and 1353.2 m asl. The vertical accuracy of the measurements was of ca. 20 mm, whereas the horizontal accuracy was ca 10 mm. From the micro-elevation maps (see following paragraph), slope maps were obtained by calculating the maximum change in elevation (in degrees) between a target cell and its eight neighbors. Low gradient values reflect a flat terrain, whereas steeper terrains are associated with higher slope values.

The EC<sub>a</sub> and micro-elevation datasets were interpolated onto 30 × 30 and 5 × 5 m grids, using ordinary kriging with a block support (Lobell et al. 2010). The following isotropic exponential semi-variogram was used to model the spatial structure of the yield data:

$$\gamma(\delta_i) = \eta + \sigma \times [1 - \exp(-h/r)] \quad (1)$$

where  $\gamma$  is the semi-variance for the variable  $\delta_i$ ,  $\eta$  represents the nugget variance,  $\sigma$  is the spatial variance component (partial sill),  $h$  is the lag distance and  $r$  is the range. The interpolations were carried out and tested with leave-one-out cross-validations using ArcMap 10.1 (ESRI, Redlands, CA, USA). Table 1 presents the fitted semi-variogram model specifications and the cross-validation errors.

The bare-soil imagery was re-sampled over the two grids in order to meet the spatial resolutions of the other datasets.

## Soil analysis

The EMI readings were analyzed using ESAP software (Lesch et al. 2000; Lesch 2005a) in order to direct soil sampling with the Response Surface Sampling Design algorithm (Lesch 2005a). Undisturbed soil cores were sampled, in the days following the EMI surveys, at 18 (F5) and 19 (F8) locations at 0–0.15, 0–0.3, 0.3–0.6, 0.6–0.9, and 0.9–1.2 m. The gravimetric water content (WC, kg kg<sup>-1</sup>) and bulk density (BD, Mg m<sup>-3</sup>) were obtained for all samples. Soil was sieved at 2 mm and analyzed for texture using the hydrometer method. The samples were then saturated and the saturation percentage (SP, %) was derived. Water was extracted from the soil saturated paste and analyzed for electrical conductivity (EC<sub>e</sub>, dS m<sup>-1</sup>) and pH (hereafter referred as pH<sub>e</sub>). Total carbon (TC, %) was analyzed with the CN2000 (LECO Corp. St. Joseph, Michigan, USA) and organic (SOC, %) carbon was analyzed with a CM5011 (UIC Inc., Rockdale, Illinois, USA) CO<sub>2</sub> coulometer.

## Yield data

Grain yield measurements were taken in early July 2003 using a Micro-Trak grain yield monitor (Micro-Trak Systems Inc., Eagle Lake, Minnesota, USA) and a DGPS. Combine harvester speed was about 2.8 (F5) and 2.6 (F8) m s<sup>-1</sup>. Raw yield data were recorded (frequency = 1 Hz) at a density of 1 measurement per 20.6 (F5) and 20.9 (F8) m<sup>2</sup>, resulting in average grain flow of 5.1 (F5) and 5.3 (F8) Mg s<sup>-1</sup>. A spatial resolution of 5 × 5 m was chosen as native resolution for the yield maps. In the raw yield data, low yield readings (<1 Mg ha<sup>-1</sup>), overlapping already harvested areas, were removed. Ordinary kriging with a 30 × 30 and 5 × 5 m block supports was used to interpolate the yield data into regular grids. Because the yield distribution was not normal, the dataset was

firstly normalized by normal score transformation (Deutsch and Journel 1992). Table 1 presents the fitted semi-variogram models specifications and the cross-validation errors.

### Landsat 7 spatial downscaling procedure

The L7 reflectance spatial downscaling (see workflow in Fig. 2) was carried out using geographically-weighted regressions (GWR) (Brunsdon et al. 1998; Fotheringham et al. 2003; Wheeler and Páez 2009) using the geophysical and terrain datasets as explanatory variables. GWR allow local variations of the equation parameters  $a$ , estimating their values at each location  $i$ . For a dependent variable  $y$  (i.e., the six L7 spectral bands) the equation reads:

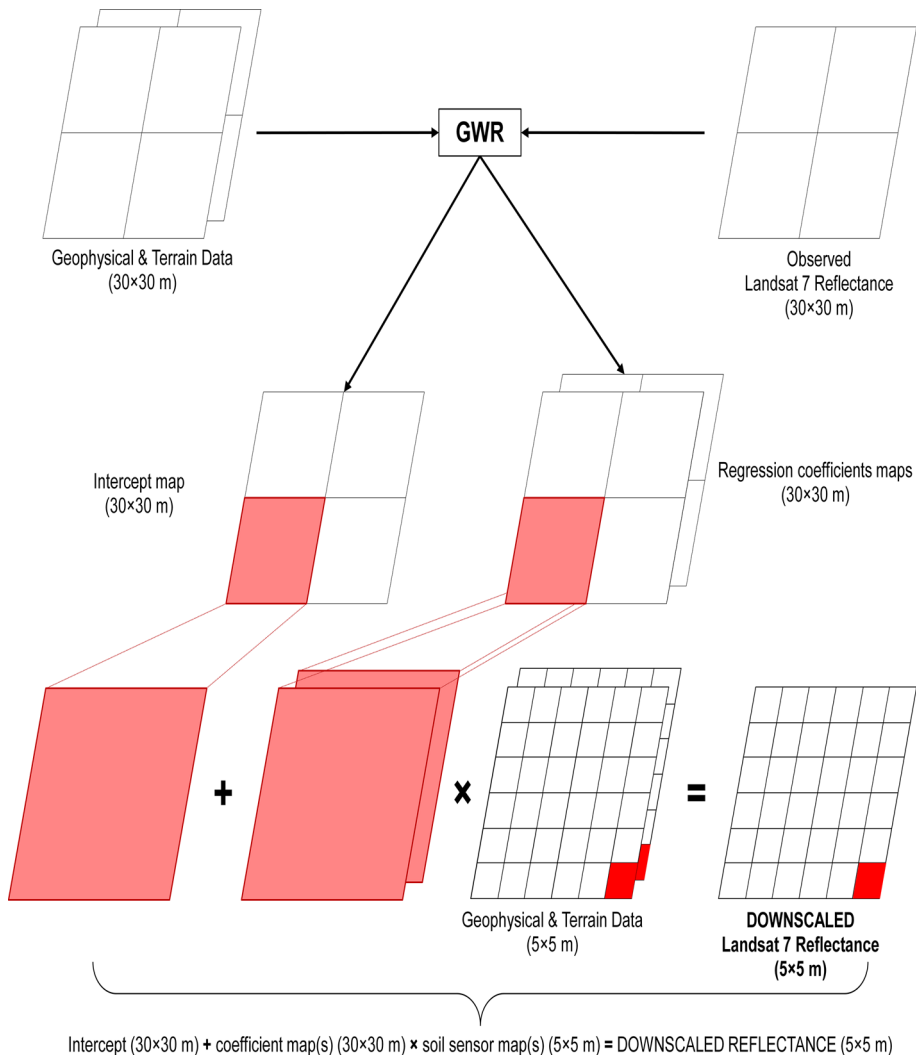


**Fig. 2** Schematic of the workflow for the Landsat 7 reflectance spatial downscaling

$$y_i = a_{i0} + \sum_k a_{ik}x_{ik} + \varepsilon_i \quad (2)$$

where  $\varepsilon_i$  is a random error term,  $a_0$  is the regression intercept, and  $a_k$  and  $x_k$  are the parameter and observed values for the  $k$ th independent (explanatory) variable. Spatial weighting is determined by incorporating all the dependent and explanatory variables falling within a geographical kernel of each target feature. The values of the regression parameters and goodness-of-fit of the GWR depend on how the kernel size is chosen (see Fotheringham et al. 2003; Wheeler and Páez 2009 for additional details). The GWR were performed with ArcMap 10.1 (ESRI, California, USA) using an adaptive kernel of neighbors. The selection of the best set of neighbors was carried out using the akaike information criterion (Akaike 1974). This process indicated that, at both fields, the best number of neighbors was 22.

The GWR technique was first used to model the relationships between L7 bands and the ancillary geophysical and terrain data at the L7 native resolution ( $30 \times 30$  m). At this step, maps for  $a_0$  and  $a_k$  were determined over the  $30 \times 30$  m grid. Secondly, these intercept and parameters maps were employed to estimate the L7 reflectance using the geophysical and terrain data, on the  $5 \times 5$  m grid, as explanatory variables (Fig. 2). In order to allow comparison of the influence of each independent variable in the GWR models, the geophysical and terrain data were standardized as follows:

$$k_{STAND,i} = \frac{k_i - \mu_k}{\sigma_k} \quad (3)$$

where  $k_{STAND,i}$  is the standardized sensor geophysical or terrain sensor reading at location  $i$ ,  $k_i$  is the sensor value at location  $i$ , and  $\mu_k$  and  $\sigma_k$  are the average and standard deviation of the considered dataset, respectively.

Similarly to traditional regression models, GWRs present issues with over-fitting when explanatory variables present multi-collinearity. Global (i.e., at field scale) multi-collinearity between variables was assessed using the variance inflation factor (VIF) (Hair et al. 1995; Mohammadi et al. 2003). In the case of multi-collinearity between explanatory variables, backward stepwise linear regressions were used to identify the best variable describing L7 reflectance, which were then used in the GWRs. The outputs of the GWRs were tested for local (i.e., within each 22-neighbors kernel) multi-collinearity of the explanatory variables using the condition number (CN) (Brunsdon et al. 2012; Fotheringham et al. 2003). The CN is the square root of the ratio between largest and smallest eigenvalues of each local regression (Fotheringham et al. 2003). Values of  $CN > 30$  indicate remarkable local collinearity between the explanatory variables used. Additionally, the regression residuals were tested for spatial autocorrelation using the Moran's I test for residual spatial autocorrelation (Cliff and Ord 1981).

### Downscaling quality assessment

The ideal validation for sharpened multi-spectral imagery would require knowing "true" reflectance at the target resolution (Rodríguez-Galiano et al. 2012; Wald et al. 1997). No reflectance data with such high spatial resolution was available for the area. Consequently, the quality of the downscaled reflectance was assessed using the yield maps. The relationships between yield and the observed L7 reflectance ( $30 \times 30$  m grid) were compared

with those of yield and the estimated L7 reflectance ( $5 \times 5$  m grid). The coefficients of determination for these relationships were compared both for ordinary least square ( $R^2$ ) and geographically-weighted ( $R^2_{GWR}$ ) regressions. For these GWRs, the bandwidth distance was assigned according to the range distances of the yield semi-variograms (Table 1). For F5 and F8, the bandwidth sizes were 60 and 39.9 m, respectively. Additionally the goodness-of-fit for the two linear regressions was compared with the normalized root mean square error (nRMSE,  $\% = \text{RMSE}/\text{range of the dependent variable as measured in the field} \times 100$ ), as the RMSE should not be used when comparing models with data sets that have different scales (i.e., different maximum, minimum and standard deviation) (Hyndman and Koehler 2006). A *Welch's t test* (Welch 1947) was used to compare the  $R^2_{OLS}$ ,  $R^2_{GWR}$ , and nRMSE for the six L7 bands at the two spatial resolutions.

**Table 2** Mean and range statistics for various soil physico-chemical properties over the 0–0.15 m depth increment of field 5 (18 locations) and field 8 (19 sampling locations)

Soil properties <sup>a</sup>	Average	Minimum	Maximum	SD	SE	Coefficient of variation	Skewness
Field 5							
WC ( $\text{kg kg}^{-1}$ )	24.34	20.23	28.14	2.28	0.54	0.09	−0.11
BD ( $\text{Mg m}^{-3}$ )	1.20	1.02	1.32	0.09	0.02	0.08	−0.38
SP (%)	42.24	35.51	53.14	4.59	1.08	0.11	0.79
Sand (%)	37.46	24.78	50.47	8.03	1.89	0.21	0.04
Silt (%)	41.63	26.57	53.50	7.72	1.82	0.19	−0.51
Clay (%)	20.91	16.64	30.15	3.53	0.83	0.17	1.14
TC (%)	0.96	0.65	1.30	0.23	0.05	0.24	0.11
SOC (%)	0.92	0.00	1.30	0.31	0.07	0.34	−1.40
IC (%)	0.04	0.00	0.65	0.15	0.04	4.24	4.24 <sup>b</sup>
pH <sub>e</sub>	6.38	5.93	7.18	0.31	0.07	0.05	0.82
EC <sub>e</sub> ( $\text{dS m}^{-1}$ )	0.61	0.31	1.29	0.27	0.06	0.45	1.04
Field 8							
WC ( $\text{kg kg}^{-1}$ )	20.24	13.49	28.36	4.50	1.03	0.22	0.20
BD ( $\text{Mg m}^{-3}$ )	1.30	1.10	1.44	0.08	0.02	0.06	−0.76
SP (%)	40.40	32.32	50.00	4.72	1.08	0.12	0.21
Sand (%)	40.17	25.46	52.14	7.00	1.61	0.17	−0.66
Silt (%)	40.60	32.72	52.83	6.15	1.41	0.15	0.79
Clay (%)	19.23	14.92	23.84	2.70	0.62	0.14	0.12
TC (%)	0.94	0.63	1.52	0.29	0.07	0.31	1.03
SOC (%)	0.88	0.62	1.50	0.26	0.06	0.30	1.31 <sup>b</sup>
IC (%)	0.06	0.00	0.74	0.18	0.04	3.25	3.51 <sup>b</sup>
pH <sub>e</sub>	7.05	6.15	7.75	0.39	0.09	0.06	−0.26
EC <sub>e</sub> ( $\text{dS m}^{-1}$ )	0.43	0.33	0.54	0.08	0.02	0.18	0.32

<sup>a</sup> WC water content, BD bulk density, SP saturation percentage, TC total carbon, SOC soil organic carbon, IC inorganic carbon, pH<sub>e</sub> pH measured from the soil saturated paste extract, EC<sub>e</sub> electrical conductivity of the the soil saturated paste extract

<sup>b</sup> Significant. Skewness is significant if skewness divided by standard error of skewness (SES) >2. SEK calculated according to Tabachnick et al. (2001)

## Results and discussion

### Soil properties and yield

Preliminary exploratory analyses indicated that the 0–0.15 m depth increment (topsoil) had the strongest correlation with yield. The two fields were characterized by similar soil properties in the topsoil profile (Table 2). In general, texture was slightly finer in F5 than F8. According to the sand content, the median soil sample at F5 was a fine loam/slit loam (sand = 34.3 %, silt = 48.7 %) whereas for F8 it was a loam, with sand = 41.92 % and

**Table 3** Correlation matrix (Pearson  $r$ ) for winter wheat yield, bare-soil (BS) orthophoto in the blue, green, red, and near-infrared (nir) bands, apparent electrical conductivity for the 0–0.75 m ( $EC_aH$ ) and 0–1.5 m ( $EC_aV$ ) soil profiles, and micro-elevation slope with various soil properties for the 0–0.15 m soil increment, at fields 5 and 8

	YIELD	BS blue	BS green	BS red	BS nir	$EC_aH$	$EC_aV$	Slope
Field 5								
WC	0.43	<b>0.57</b>	<b>0.58</b>	<b>0.60</b>	<b>0.57</b>	<b>-0.52</b>	-0.41	-0.21
BD	-0.20	<b>-0.65</b>	<b>-0.66</b>	<b>-0.71</b>	<b>-0.70</b>	0.42	-0.03	<b>0.52</b>
SP	0.03	0.35	0.34	0.39	0.31	-0.30	-0.28	-0.14
Sand	<b>-0.56</b>	<b>-0.85</b>	<b>-0.83</b>	<b>-0.88</b>	<b>-0.82</b>	<b>0.73</b>	0.17	<b>0.72</b>
Silt	<b>0.70</b>	<b>0.84</b>	<b>0.85</b>	<b>0.88</b>	<b>0.83</b>	<b>-0.89</b>	-0.34	<b>-0.71</b>
Clay	-0.26	0.10	0.03	0.07	0.05	0.29	0.35	-0.08
TC	<b>0.51</b>	<b>0.82</b>	<b>0.82</b>	<b>0.85</b>	<b>0.81</b>	<b>-0.71</b>	-0.46	<b>-0.49</b>
SOC	<b>0.55</b>	<b>0.68</b>	<b>0.68</b>	<b>0.71</b>	<b>0.64</b>	<b>-0.63</b>	<b>-0.51</b>	-0.36
IC	-0.37	-0.18	-0.19	-0.19	-0.12	0.24	0.37	0.01
$pH_e$	<b>-0.47</b>	-0.29	-0.29	-0.34	-0.33	0.46	-0.03	<b>0.47</b>
$EC_c$	0.03	0.17	0.23	0.19	0.24	0.00	0.07	-0.03
YIELD	-	<b>0.59</b>	<b>0.58</b>	<b>0.55</b>	<b>0.61</b>	<b>-0.86</b>	-0.35	<b>-0.61</b>
Field 8								
WC	0.29	0.27	0.23	0.30	0.25	-0.32	-0.31	-0.10
BD	-0.33	<b>-0.51</b>	-0.45	-0.45	<b>-0.47</b>	0.21	0.29	-0.15
SP	0.06	-0.02	-0.05	-0.05	-0.04	0.35	-0.10	0.25
Sand	<b>-0.50</b>	<b>-0.47</b>	-0.42	-0.38	-0.43	0.20	<b>0.46</b>	0.17
Silt	<b>0.60</b>	<b>0.53</b>	<b>0.48</b>	0.44	<b>0.49</b>	<b>-0.46</b>	<b>-0.48</b>	-0.25
Clay	-0.08	-0.01	-0.02	-0.02	-0.02	0.45	-0.09	0.11
TC	0.35	0.45	0.41	0.39	0.42	-0.23	-0.33	0.14
SOC	<b>0.62</b>	<b>0.70</b>	<b>0.65</b>	<b>0.62</b>	<b>0.67</b>	<b>-0.48</b>	<b>-0.60</b>	-0.12
IC	-0.33	-0.30	-0.28	-0.28	-0.30	0.33	0.35	0.39
$pH_e$	-0.23	-0.17	-0.16	-0.21	-0.22	<b>0.53</b>	0.06	0.10
$EC_c$	-0.17	-0.31	-0.28	-0.32	-0.30	0.28	<b>0.52</b>	0.12
YIELD	-	<b>0.69</b>	<b>0.66</b>	<b>0.67</b>	<b>0.66</b>	<b>-0.77</b>	<b>-0.48</b>	<b>-0.56</b>

Bold numbers are significant at the  $p < 0.05$  level

WC water content, BD bulk density, SP saturation percentage, TC total carbon, SOC soil organic carbon, IC inorganic carbon,  $pH_e$  pH measured from the soil saturated paste extract,  $EC_c$  electrical conductivity of the soil saturated paste extract

silt = 17.89 %. Both F5 and F8 were characterized by organic carbon contents smaller than 1.5 %. Measured  $EC_e$  for the two fields indicated non-saline soils ( $<2 \text{ dS m}^{-1}$ ).

Wheat yields were similar in the two fields, with an average grain yield of 2.3 and 2.6  $\text{Mg ha}^{-1}$  for field 5 and 8, respectively (Table 1). In both fields, yield was significantly influenced by texture, soil carbon and, in field 5 only, by  $pH_e$  (Table 3). Soil carbon was highly correlated ( $p < 0.05$ ) with sand and silt content in both fields, with  $r = -0.74$  and 0.78 in F5 and  $r = -0.78$  and 0.83 in F8. As expected in soils with low organic carbon content, such organic fraction was associated with the finer texture (Lugato et al. 2009). Additionally, in F5,  $pH_e$  was significantly correlated with silt ( $r = -0.51$ ). It is, therefore, reasonable to assume that the main factor influencing yield spatial variability was soil texture. Rainfall was scarce in the 2002–2003 growing season (287 mm), so crop growth was limited by water availability. The WC was significantly ( $p < 0.05$ ) correlated with sand ( $r = -0.57$ ) and silt ( $r = 0.60$ ) in F5. For F8, relationships were similar yet not highly significant ( $p < 0.1$ ).

### Geophysical and terrain sensor data

Geophysical and terrain sensor measurements helped to describe the spatial variability of yield in the two fields. Both  $EC_aH$  and bare-soil imagery were significantly ( $p < 0.05$ ) correlated with sand, silt and soil carbon content (Table 3). Micro-elevation slope in F5 was significantly correlated with silt, sand and total carbon contents, and with  $pH_e$ . These relationships were not significant in F8. However, micro-elevation slope was negatively correlated ( $p < 0.05$ ) with yield for both fields (Table 3), indicating that the flatter the terrain the higher the yield. The higher observed yield in level terrain was likely due to increased water availability (Moore et al. 1993; Peterson et al. 1993; Kravchenko et al. 2002).

The  $EC_aH$  values (Table 1) were low at both fields ( $<0.35 \text{ dS m}^{-1}$ ), as one would expect in non-saline soils (Scudiero et al. 2013). The correlations of  $EC_a$  in both fields was positively correlated with sand, and negatively correlated with silt and yield (Table 3). These observations were consistent with those reported by Johnson et al. (2003a) for winter wheat (in 1999) and maize (in 2000) in the same fields. Johnson et al. (2003a) measured  $EC_a$  in 1999 from resistivity readings obtained with a Veris 3100 Sensor Cart (Geoprobe Syst., Salina, Kansas, USA) over the 0–0.3 and 0–0.9 m soil profiles. Their  $EC_a$  measurements were also negatively correlated with yield and silt. Moreover, they observed that the shallow measurements best reflected yield for both crops. The Veris 3100  $EC_a$  measurements at 0–0.3 m taken in 1999 were significantly correlated with EM 38  $EC_aH$  measurements taken in 2005 at the soil sampling locations with  $r = 0.69$  and 0.64 in F5 and F8, respectively, indicating that spatial patterns in  $EC_a$  generally remain stable over time.

The bare soil imagery (blue, green, red, and near-infrared bands) and the  $EC_aH$  data were collinear according to the variance inflation factor. Indeed, both measurements were highly correlated with spatial changes in texture. This collinearity between the two geophysical measurements is, in geographical terms, a local phenomenon. Indeed, the use of sensors to characterize soil spatial variability is an empirical practice, even though based on physical relationships between soil and sensor measurements. The relationships between soil properties and sensor readings vary across regions, with apparent electrical conductivity being used to map (regional-scale) soil salinity in the western USA (Corwin and Lesch 2014; Lesch 2005b) and (regional-scale) texture in the central USA (Harvey and Morgan 2009). Consequently, different regions require the use of different sensors:

Scudiero et al. (2013) used  $EC_a$  and bare-soil reflectance to monitor yield spatial variability in a delta plain affected by saltwater intrusion and contrasting soil properties in Italy; Triantafyllis et al. (2009) used  $EC_a$  and bare-soil imagery to classify a strongly sodic irrigated field with contrasting lithography in Australia; Priori et al. (2013b) improved the harvest quality of wine through harvest zoning in Italy using a combination of  $EC_a$ , bare-soil imagery and micro-elevation data. Conversely, in this work, bare-soil imagery data were discarded due to collinearity with  $EC_aH$ . Indeed, exploratory backward multiple linear regressions indicated that  $EC_aH$  was a better independent variable than any bare-soil imagery bands, in either field. Moreover,  $EC_aV$  did not describe variations in canopy reflectance for the two fields. Finally, for both fields,  $EC_aH$  and micro-elevation slope were chosen as independent variables for the GWR model.

### Downscaling Landsat 7 reflectance

As a first step in the downscaling procedure, the spatial variability of the six L7 spectral bands was described with GWRs using  $EC_aH$  and micro-elevation slope maps as explanatory variables (Table 4). All the GWRs were characterized by CN maps with values smaller than 30, indicating that local collinearity between explanatory variables was not significant (Brunsdon et al. 2012; Fotheringham et al. 2003). Moreover, the residuals of the regression did not show significant spatial autocorrelation.

For both fields, use of a multi-sensor platform described a high fraction of the spatial variability in L7 canopy reflectance with high  $R^2$  and low RMSE values, in all six spectral

**Table 4** Landsat 7 observed data and geographically-weighted regression (GWR) specifications

Spectral band <sup>a</sup>	Observed data (reflectance %)			GWR specifications			
	Average	Minimum	Maximum	Explanatory variables <sup>b</sup>	$R^2$	RMSE <sup>c</sup> (%)	
Field 5							
B	8.8	7.9	9.6	$EC_aH$ Slope	0.89	0.11	
G	11.4	10.2	12.4	$EC_aH$ Slope	0.93	0.13	
R	14.0	12.4	15.5	$EC_aH$ Slope	0.94	0.18	
NIR	24.8	23.5	27.0	$EC_aH$ Slope	0.89	0.22	
IR1	32.6	30.3	34.8	$EC_aH$ Slope	0.91	0.23	
IR2	25.9	22.8	28.3	$EC_aH$ Slope	0.92	0.29	
Field 8							
B	8.7	7.7	9.5	$EC_aH$ Slope	0.85	0.12	
G	11.2	9.9	12.2	$EC_aH$ Slope	0.87	0.15	
R	13.6	11.4	15.2	$EC_aH$ Slope	0.87	0.22	
NIR	24.8	22.9	28.6	$EC_aH$ Slope	0.83	0.34	
IR1	32.0	28.9	34.4	$EC_aH$ Slope	0.88	0.28	
IR2	25.6	21.9	27.6	$EC_aH$ Slope	0.86	0.35	

<sup>a</sup> B blue (450–520 nm), G green (520–600 nm), R red (630–690 nm), NIR near-infrared (770–900 nm), IR1 shortwave infrared 1 (1550–1750 nm), and IR2 shortwave infrared 2 (2090–2350 nm)

<sup>b</sup>  $EC_aH$  apparent electrical conductivity for the 0–0.75 cm soil profile, and Slope, micro-elevation slope

<sup>c</sup> RMSE root mean square error

bands. Generally, the B and NIR bands were characterized by the lowest observed-estimated  $R^2$  values (Table 4). The GWR provided stronger relationships at F5 than F8 with average  $R^2$  of 0.91 and 0.86 and RMSE of 0.19 and 0.25 %, respectively. The slight difference in goodness-of-fit between the two fields could indicate that: (i) soil properties described by the sensor data influence crop health more in F5 than in F8; (ii) L7 reflectance-wheat health relationships are stronger in F5 than F8 (e.g., no biasing influences from weeds in F5); or (iii) a combination of the two. One way to analyze this difference could be through local  $R^2$  maps of the observed L7 reflectance versus the explanatory variables (not shown). These maps can be used as indicators of the extent of the influence of the described soil properties on crop growth: low local  $R^2$  values would suggest that other soil properties or non-edaphic factors might play (locally) an important role on influencing crop growth.

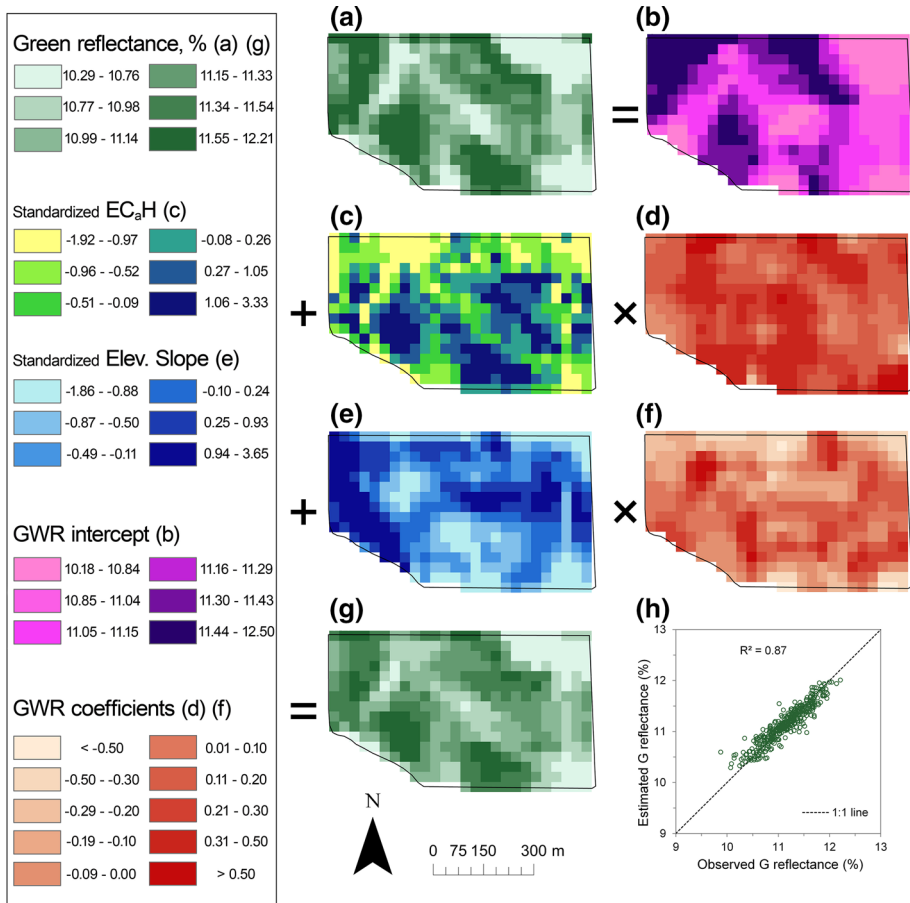


**Fig. 3** Geographically-weighted regression (GWR) for the **a** green band of Landsat 7 at field 8. The **g** estimated reflectance is calculated using the maps of **b** the GWR intercept, **c** apparent electrical conductivity of the 0–0.75 m soil profile ( $EC_{aH}$ ), **d** the GWR coefficient for  $EC_{aH}$ , **e** micro-elevation slope, and **f** the GWR coefficient for micro-elevation slope. The observed versus estimated relationship is reported in **(h)** (Color figure online)

Figure 3 depicts the GWR for the G band in F8. This field was chosen over F5 because the range of reflectance values was wider (Table 3). The choice of the G band was arbitrary, as data from all spectral bands showed highly significant ( $p > 0.01$ ) Pearson correlations (not shown). Observed (Fig. 3a) and estimated (Fig. 3g) G reflectance showed similar spatial patterns. The two maps were characterized by similar average values (both ca. 11.16 %), but had different minimum (10.07 and 10.29 % for the observed and estimated, respectively) and maximum (12.21 and 12.01 % for the observed and estimated, respectively) reflectance values. The observed:estimated relationship was characterized by fairly high  $R^2 = 0.87$  and low RMSE = 0.15 % (Fig. 3h).

The maps for intercept (Fig. 3b), and  $EC_aH$  and micro-elevation slope coefficients (Fig. 3d, f, respectively), were generated using the GWR process for each L7 band, in both fields. It is clear from the  $EC_aH$  and micro-elevation slope coefficient maps that the influence of soil properties (i.e., those represented by these two sensors) on canopy reflectance varied greatly across fields. The coefficient maps (Fig. 3d, f) might help quantify the influence of each independent variable on the dependent variable across each field. This can be useful for multiple purposes, such as identifying areas affected by a particular soil-related stress or nutrient deficiency. In the example,  $EC_aH$  influence in the GWR was generally (ca. 77 % of times) greater than micro-elevation slope. The coefficient map values ranged from  $-0.26$  to  $1.09$ , and  $-0.64$  to  $0.63$  for  $EC_aH$  and micro-elevation

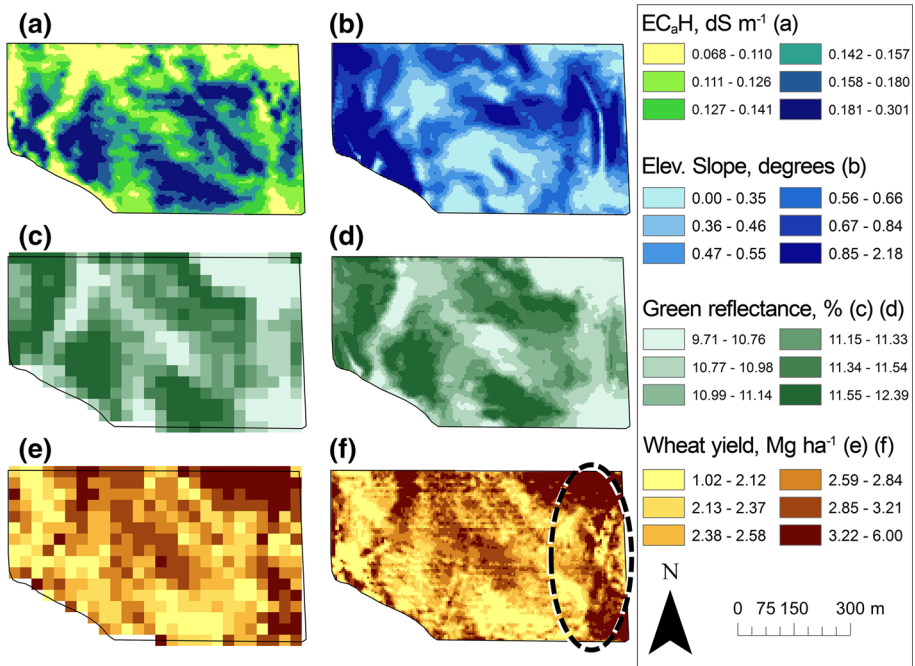


**Fig. 4** Maps for **a** apparent electrical conductivity of the 0–0.75 m soil profile ( $EC_aH$ ) at  $5 \times 5$  m, **b** micro-elevation slope at  $5 \times 5$  m, **c** the observed (at  $30 \times 30$  m) and **d** downsampled (at  $5 \times 5$  m) Landsat 7 reflectance in the *green band*, and wheat yield maps at **e**  $30 \times 30$  m and **f**  $5 \times 5$  m, in field 8. The *dashed selection* in **f** highlights a portion of the field characterized by contrasting changes in grain yield over short distances (Color figure online)

slope, respectively; the lower the coefficient value at each pixel, the lower the (local) influence in describing L7 reflectance.

Once the coefficient maps were obtained for all L7 bands, they were used to model downscaled values of L7 reflectance at the target resolution of  $5 \times 5$  m grid. The  $30 \times 30$  m coefficient maps were employed to estimate the reflectance over the thirty-six  $5 \times 5$  m cells included in each of their pixels, as shown in Fig. 2. The EC<sub>a</sub>H, micro-elevation slope, and downscaled G reflectance for F8 are shown in Fig. 4 a, b, d, respectively. Figure 4a, b shows very similar yet non-identical spatial patterns. Indeed, the two variables were not collinear and their Pearson relationship was weak ( $r = 0.11$ ). Figure 4d resembles the observed L7 G data (Fig. 4c) yet with spatial patterns and scale of variation observed in Fig. 4a, b. The observed and the downscaled G reflectance at F8 were characterized by different minimum (10.07 and 9.71 %, respectively), maximum (12.21 and 12.39 %, respectively) and standard deviation (0.42 and 0.39 %, respectively), but were characterized by very similar average reflectance (11.16 and 11.13 %, respectively).

### Quality assessment of the downscaled L7 canopy reflectance

The ordinary least square coefficients of determination ( $R^2_{OLS}$ ) between yield and L7 reflectance at the native (i.e., over the  $30 \times 30$  m grid) resolution are reported in Table 5. For both fields, NIR reflectance was not significantly correlated with yield; therefore, the ( $R^2_{OLS}$ ) and nRMSE values are not reported. Overall, larger ( $R^2_{OLS}$ ) values were observed for F8 than F5 (Table 5). Based solely on ( $R^2_{OLS}$ ) values, this could suggest two things: (i)

**Table 5** Ordinary least square coefficient of determination ( $R^2$ ) and normalized root mean square error (nRMSE) and geographically-weighted coefficient of determination ( $R^2_{GWR}$ ) between the observed ( $30 \times 30$  m) and downscaled ( $5 \times 5$  m) Landsat 7 (L7) reflectance with the winter wheat yield at the two spatial scales, at the two fields

L7 Band <sup>a</sup>	$R^2$		nRMSE (%)		$R^2_{GWR}$	
	$30 \times 30$ m	$5 \times 5$ m	$30 \times 30$ m	$5 \times 5$ m	$30 \times 30$ m	$5 \times 5$ m
Field 5						
B	0.27	0.28	11.37	7.33	0.83	0.84
G	0.25	0.26	11.50	7.34	0.88	0.87
R	0.26	0.26	11.43	7.33	0.89	0.86
NIR	ns	ns	ns	ns	0.81	0.70
IR1	0.20	0.21	11.85	7.59	0.87	0.84
IR2	0.24	0.25	11.61	7.38	0.87	0.84
Field 8						
B	0.37	0.43	13.20	9.22	0.85	0.85
G	0.42	0.44	12.60	13.92	0.88	0.84
R	0.35	0.41	13.42	10.07	0.87	0.84
NIR	ns	ns	ns	ns	0.85	0.87
IR1	0.26	0.34	14.29	9.93	0.88	0.89
IR2	0.42	0.47	12.63	8.84	0.89	0.87

<sup>a</sup> B blue (450–520 nm); G green (520–600 nm), R red (630–690 nm), NIR near-infrared (770–900 nm), IR1 shortwave infrared 1 (1550–1750 nm), and IR2 shortwave infrared 2 (2090–2350 nm)

ns omitted because ordinary least square regression was non-significant

in F8, the yield-reflectance relationships were stronger than in F5; or (ii) the yield-L7 relationships are of equal strength in both fields but the ordinary least square approach does not sufficiently describe them. Indeed, when the geographically-weighted coefficients of determination ( $R_{GWR}^2$ ) at the native spatial scale ( $30 \times 30$  m) were considered, reflectance-yield relationships for the two fields were of approximately the same magnitude (Table 5). Moreover, the NIR-yield relationships were characterized by  $R_{GWR}^2$  values similar in size to those of the other five spectral bands. This suggests that the localized approach provided by GWRs greatly improves the ability to describe spatial plant-soil relationships, compared to the ordinary least squares approach.

The criterion adopted to assess the quality of downscaled L7 reflectance was the following: if the strength of the relationships between L7 canopy reflectance and wheat yield, at the  $5 \times 5$  m resolution, were of similar (or greater) strength than those at the  $30 \times 30$  m resolution, then the downscaled reflectance would be considered “acceptable”. The t-test indicated that the  $R^2$  and  $R_{GWR}^2$  values between yield and all six spectral bands, across the two fields, were not significantly different at the two spatial scales. Nevertheless, the downscaled L7 reflectance was always characterized by higher  $R^2$  values with yield than that of observed data at  $30 \times 30$  m (Table 5). On average, the downscaling procedure increased the yield-reflectance ordinary least squares relationships by 3.2 %. The nRMSE values of the downscaled L7 reflectance for the six bands were significantly ( $p < 0.01$ ) lower than those at the native spatial resolution, with an average improvement across the two fields of 3.49 % (Table 5). These observations indicate that the downscaled L7 reflectance quality is comparable (or slightly better) than that at  $30 \times 30$  m.

The maps of wheat yield at  $30 \times 30$  m (Fig. 4e) and  $5 \times 5$  m (Fig. 4f) were characterized by similar average values ( $2.63$  and  $2.65$   $\text{Mg ha}^{-1}$ , respectively). Figure 4f was characterized by lower minimum =  $1.02$   $\text{Mg ha}^{-1}$  ( $1.18$   $\text{Mg ha}^{-1}$  for the  $30 \times 30$  m map) and higher maximum =  $6.00$   $\text{Mg ha}^{-1}$  ( $4.73$   $\text{Mg ha}^{-1}$  for the  $30 \times 30$  m map) yield values, and higher standard deviation =  $0.61$   $\text{Mg ha}^{-1}$  ( $0.59$   $\text{Mg ha}^{-1}$  for the  $30 \times 30$  m map). The quality of the L7 downscaling procedure was remarkable: patterns in the downscaled G band (Fig. 4d) were very similar to those of the yield map at the  $5 \times 5$  m resolution (Fig. 4f). It is clear that the reflectance downscaling procedure allows for the characterization of spatial variability in crop status/yield at a very high spatial resolution, with detailed accuracy. This was particularly evident in areas of the field where grain yield changed dramatically within short distances, such as the eastern side of the field (dashed selection in Fig. 4f). Little small scale variation was captured by the native L7 reflectance map (Fig. 4c), whereas it was well described by the downscaled maps (Fig. 4d).

## Using downscaled reflectance

Monitoring crop health at the farm scale (e.g., hundreds of hectares) at high spatial resolution is still a challenge for farmers, land resource managers, agriculture consultants, and extension specialists. Remote sensing can be used effectively to monitor crop health during the growing season and therefore address site-specific agronomic practices. High resolution data is needed to fully understand and address crop spatial variability. However, high spatial resolution comes at a very high price. For example,  $2 \times 2$  m multi-spectral imagery would cost, for a  $25 \times 25$  km farmland, at least 2000 USD (as of May 2015) per acquisition. The methodology proposed herein can be used to monitor plant-soil relationships at a very-high spatial resolution using free satellite data and maps of soil sensors. The high resolution sensor maps required for the procedure (and advisable for most site-specific

practices) are generally only necessary to establish initial soil patterns of spatial variability. As discussed above for  $EC_a$ , spatial patterns of soil properties, especially those related to and influenced by soil texture, tend to be very stable in time under consistent agricultural management practices. The downscaling service could be offered, at the farm scale, by agricultural consultants and extension agents, or, at a larger scale, by Natural Resource Conservation Service field staff (or equivalent, outside the USA) in order to aid decision making of producers and natural resource managers.

## Conclusions

In this manuscript, a spatial statistics approach to sharpen Landsat 7 canopy reflectance data from its native resolution of  $900\text{--}25\text{ m}^2$  (or higher) using spatial information provided by multiple soil (i.e., geophysical and terrain) sensors is presented. A geographically-weighted regression described large portions of the spatial variability ( $R^2$  range 0.83–0.94) of Landsat 7 canopy reflectance in all six (visible to infrared) spectral bands using maps of soil apparent conductivity and micro-elevation slope as independent variables. The results provided reliable high spatial resolution reflectance that may be used for precision agriculture practices at the farm scale. In fact, the relationships between Landsat 7 reflectance and yield maps (used as ground truth for assessing the quality of the downscaling procedure) were similar (or improved) using high resolution simulated reflectance, as opposed to the original  $900\text{ m}^2$  resolution Landsat 7 data. The quality of the downscaled procedure depended on: (a) the selection of appropriate soil sensors that accurately reflect spatial variability in those soil properties that influence crop health/yield (texture, soil carbon content and  $pH_e$ ), and (b) the accurate measurement of crop status (with little to no biasing effects from other non-edaphic factors, such as weed pressure) by Landsat 7 reflectance.

This methodology should be tested using multi-year studies in crop status spatio-temporal variability. Different meteorological settings across years can alter the spatial patterns of plant-soil relationships and different crops can show varying spatial patterns in yield over the same field. As a matter of fact, Northeast Colorado was in the throes of a severe drought during the time period covered in this paper. Yields were remarkably below average. At the time, average yields for the sites were around  $2.5\text{ Mg ha}^{-1}$  while in a good year they could exceed  $3.8\text{ Mg ha}^{-1}$ . However, spatial patterns in soil properties described by soil sensors do not generally change in short time periods (e.g., 5–7 years). Thus, the same multi-sensor platform could be used for several years, to provide highly accurate downscaled L7 reflectance because the geographically-weighted regression technique allows for local changes in each regressor coefficient.

Clearly this manuscript and others highlight the benefits of using multiple sensors to characterize spatial variability in soil–plant relationships at farm scale. Often though, only a single sensor is used to carry out precision agricultural practices (e.g., modeling yield, delineating site-specific management zones and optimizing soil sampling designs) with no guarantee that all relevant soil properties are actually represented/sensed. More research is needed to investigate the benefits of using multiple sensor platforms in precision agriculture in order to define, by geographical region, which sensor measurements are most useful for improving soil and crop management.

**Acknowledgments** The authors thank Kevin Yemoto and Clay Wilkinson for their technical support in the field and laboratory; and Harry Forster and Nahid Visteh for their technical laboratory support; as well as the following students for their assistance in soil sample preparation and routine physical and chemical soil

analyses: Derrick Lai, Linda Lam, Jon Edwards, and Jennifer Palarca. The authors are especially indebted to Matt Johnson and the late Russ Johnson for the use of their land and for managing day-to-day farm operations, which made the project possible.

## References

- Adamchuk, V. I., Hummel, J., Morgan, M., & Upadhyaya, S. (2004). On-the-go soil sensors for precision agriculture. *Computers and Electronics in Agriculture*, *44*, 71–91.
- Akaike, H. (1974). A new look at the statistical model identification. *IEEE Transactions on Automatic Control*, *19*, 716–723.
- Blackmer, T., Schepers, J., & Meyer, G. (1995). Remote sensing to detect nitrogen deficiency in corn. *Proceedings of second international conference in site-specific management for agricultural systems*. ASA, CSSA, SSSA, Madison, WI, pp. 505–512.
- Blackmore, S. (1999). Remedial correction of yield map data. *Precision Agriculture*, *1*, 53–66.
- Brunsdon, C., Fotheringham, S., & Charlton, M. (1998). Geographically weighted regression. *Journal of the Royal Statistical Society: Series D (The Statistician)*, *47*, 431–443.
- Braga, F., Morari, F., Rizzetto, F., Scudiero, E., Teatini, P., & Tosi, L. et al. (2012). Characterizing the saltwater effect on soil productivity by WorldView-2 images in the southern margin of the Venice Lagoon, Italy. In Scappini, S., & Zapparoli, S. (Eds.), 7th EUREGEO, European Congress on Regional Geoscientific Cartography and Information Systems, Centro Stampa Regione Emilia-Romagna, Bologna, I: pp. 361–362.
- Brunsdon, C., Charlton, M., & Harris, P. (2012). Living with collinearity in local regression models. In Vieira, C., Bogorny, V., Aquino, A. R. (Eds.) *Proceedings of the 10th international symposium on spatial accuracy assessment in natural resources and environmental sciences*. ISARA, Florianópolis, Retrieved June 16, 2015 from <http://www.spatial-accuracy.org/BrunsdonAccuracy2012>.
- Chang, C. W., Mausbach, M. J., Laird, D. A., & Hurburgh, C. R. (2001). Near-infrared reflectance spectroscopy—Principal components regression analyses of soil properties. *Soil Science Society of America Journal*, *65*, 480–490.
- Cliff, A. D., & Ord, J. K. (1981). *Spatial processes: Models & applications*. London: Pion.
- Corwin, D. L., & Lesch, S. M. (2005). Characterizing soil spatial variability with apparent soil electrical conductivity: I. Survey protocols. *Computers and Electronics in Agriculture*, *46*, 103–133.
- Corwin, D. L., & Lesch, S. M. (2010). Delineating site-specific management units with proximal sensors. In M. O. Oliver (Ed.), *Geostatistical applications for precision agriculture* (pp. 139–165). New York, NY: Springer.
- Corwin, D. L., & Lesch, S. M. (2014). A simplified regional-scale electromagnetic induction—Salinity calibration model using ANOCOVA modeling techniques. *Geoderma*, *230–231*, 288–295.
- Corwin, D. L., Lesch, S. M., Shouse, P., Soppe, R., & Ayars, J. (2003). Identifying soil properties that influence cotton yield using soil sampling directed by apparent soil electrical conductivity. *Agronomy Journal*, *95*, 352–364.
- Deutsch, C. V., & Journel, A. G. (1992). *Geostatistical software library and user's guide*. New York, NY: Oxford University Press.
- Ellis, S., & Mellor, T. (2002). *Soils and environment*. London: Routledge.
- Fotheringham, A. S., Brunsdon, C., & Charlton, M. (2003). *Geographically weighted regression: The analysis of spatially varying relationships*. Chichester, Hoboken, NJ: Wiley.
- Hair, J. F., Jr, Anderson, R. E., Tatham, R. L., & Black, W. C. (1995). *Multivariate data analysis with readings* (pp. 130–133). New Jersey: Prentice Hall.
- Harvey, O. R., & Morgan, C. L. (2009). Predicting regional-scale soil variability using a single calibrated apparent soil electrical conductivity model. *Soil Science Society of America Journal*, *73*, 164–169.
- Hyndman, R. J., & Koehler, A. B. (2006). Another look at measures of forecast accuracy. *International Journal of Forecasting*, *22*, 679–688.
- Iqbal, J., Read, J. J., Thomasson, A. J., & Jenkins, J. N. (2005). Relationships between soil–landscape and dryland cotton lint yield. *Soil Science Society of America Journal*, *69*, 872–882.
- Johnson, C. K., Drijber, R. A., Wienhold, B. J., & Doran, J. W. (2008). Productivity zones based on bulk soil electrical conductivity. In B. J. Allred, B. J. Allred, J. J. Daniels, & M. R. Ehsani (Eds.), *Handbook of agricultural geophysics* (pp. 263–272). New York, NY: CRC Press, Taylor & Francis Group.
- Johnson, C. K., Eskridge, K. M., Wienhold, B. J., Doran, J. W., Peterson, G. A., & Buchleiter, G. W. (2003a). Using electrical conductivity classification and within-field variability to design field-scale research. *Agronomy Journal*, *95*, 602–613.

- Johnson, C. K., Mortensen, D. A., Wienhold, B. J., Shanahan, J. F., & Doran, J. W. (2003b). Site-specific management zones based on soil electrical conductivity in a semiarid cropping system. *Agronomy Journal*, *95*, 303–315.
- Kravchenko, A., Bollero, G., Omonode, R., & Bullock, D. (2002). Quantitative mapping of soil drainage classes using topographical data and soil electrical conductivity. *Soil Science Society of America Journal*, *66*, 235–243.
- Kravchenko, A., & Robertson, G. (2007). Can topographical and yield data substantially improve total soil carbon mapping by regression kriging? *Agronomy Journal*, *99*, 12–17.
- Lesch, S. (2005a). Sensor-directed response surface sampling designs for characterizing spatial variation in soil properties. *Computers and Electronics in Agriculture*, *46*, 153–179.
- Lesch, S. (2005b). Statistical techniques for calibrating regional (multi-field) EM survey data. In *Proceedings of the international salinity forum, managing saline soils and water: science, technology, and soil issues*. USDA-ARS, U.S. Salinity Laboratory, Riverside, CA, pp. 289–292.
- Lesch, S.M., Rhoades, J.D. & Corwin, D.L. (2000). ESAP-95 version 2.01 R. User manual and tutorial guide. Research Rpt 146. USDA-ARS, U.S. Salinity Laboratory, Riverside, CA.
- Lobell, D. B., Asner, G. P., Ortiz-Monasterio, J. I., & Benning, T. L. (2003). Remote sensing of regional crop production in the Yaqui Valley, Mexico: estimates and uncertainties. *Agriculture, Ecosystems & Environment*, *94*, 205–220.
- Lobell, D. B., Lesch, S. M., Corwin, D. L., Ulmer, M. G., Anderson, K. A., Potts, D. J., et al. (2010). Regional-scale assessment of soil salinity in the Red River Valley using multi-year MODIS EVI and NDVI. *Journal of Environmental Quality*, *39*, 35–41.
- Lugato, E., Morari, F., Nardi, S., Berti, A., & Giardini, L. (2009). Relationship between aggregate pore size distribution and organic-humic carbon in contrasting soils. *Soil Tillage Research*, *103*, 153–157.
- Martini, E., CoMina, C., Priori, S., & CoStantini, E. (2013). A combined geophysical-pedological approach for precision viticulture in the Chianti hills. *Bollettino di Geofisica Teorica ed Applicata*, *54*, 165–181.
- Masek, J. G., Vermote, E. F., Saleous, N. E., Wolfe, R., Hall, F. G., Huemmrich, K. F., et al. (2006). A Landsat surface reflectance dataset for North America, 1990–2000. *IEEE Geoscience and Remote Sensing Letters*, *3*, 68–72.
- Mohammadi, S., Prasanna, B., & Singh, N. (2003). Sequential path model for determining interrelationships among grain yield and related characters in maize. *Crop Sciences*, *43*, 1690–1697.
- Moore, I. D., Gessler, P., Nielsen, G., & Peterson, G. (1993). Soil attribute prediction using terrain analysis. *Soil Science Society of America Journal*, *57*, 443–452.
- Mulla, D. J. (2013). Twenty five years of remote sensing in precision agriculture: Key advances and remaining knowledge gaps. *Biosystems Engineering*, *11*, 358–371.
- Peterson, G., Westfall, D., & Cole, C. (1993). Agroecosystem approach to soil and crop management research. *Soil Science Society of America Journal*, *57*, 1354–1360.
- Ping, J., & Dobermann, A. (2005). Processing of yield map data. *Precision Agriculture*, *6*, 193–212.
- Priori, S., Fantappiè, M., Magini, S., & Costantini, E. (2013a). Using the ARP-03 for high-resolution mapping of calcic horizons. *International Agrophysics*, *27*, 313–321.
- Priori, S., Martini, E., Andrenelli, M., Magini, S., Agnelli, A., Bucelli, P., et al. (2013b). Improving wine quality through harvest zoning and combined use of remote and soil proximal sensing. *Soil Science Society of America Journal*, *77*, 1338–1348.
- Rodriguez-Galiano, V., Pardo-Iguzquiza, E., Sanchez-Castillo, M., Chica-Olmo, M., & Chica-Rivas, M. (2012). Downscaling Landsat 7 ETM thermal imagery using land surface temperature and NDVI images. *International Journal of Applied Earth Observation and Geoinformation*, *18*, 515–527.
- Savabi, M., Scully, B., Strickland, T., Sullivan, D., & Hubbard, R. (2013). Use of statistical and conceptual path models to predict corn yields across management-zones on the southeast coastal plain. *Journal of Agricultural Science*, *1*, 32–51.
- Schepers, A. R., Shanahan, J. F., Liebig, M. A., Schepers, J. S., Johnson, S. H., & Luchiari, A. (2004). Appropriateness of management zones for characterizing spatial variability of soil properties and irrigated corn yields across years. *Agronomy Journal*, *96*, 195–203.
- Schmidt, F., & Persson, A. (2003). Comparison of DEM data capture and topographic wetness indices. *Precision Agriculture*, *4*, 179–192.
- Scudiero, E., Skaggs, T. H., & Corwin, D. L. (2014a). Regional scale soil salinity evaluation using landsat 7, western San Joaquin Valley, California, USA. *Geoderma Regional*, *2–3*, 82–90.
- Scudiero, E., Teatini, P., Corwin, D. L., Deiana, R., Berti, A., & Morari, F. (2013). Delineation of site-specific management units in a saline region at the Venice Lagoon margin, Italy, using soil reflectance and apparent electrical conductivity. *Computers and Electronics in Agriculture*, *99*, 54–64.

- Scudiero, E., Teatini, P., Corwin, D. L., Ferro, N. D., Simonetti, G., & Morari, F. (2014b). Spatio-temporal response of maize yield to edaphic and meteorological conditions in a saline farmland. *Agronomy Journal*, *106*, 2163–2174.
- Shanahan, J. F., Schepers, J. S., Francis, D. D., Varvel, G. E., Wilhelm, W. W., Tringe, J. M., et al. (2001). Use of remote-sensing imagery to estimate corn grain yield. *Agronomy Journal*, *93*, 583–589.
- Tabachnick, B. G., Fidell, L. S., & Osterlind, S. J. (2001). *Using multivariate statistics*. Boston, MA: Allyn and Bacon.
- Triantafyllis, J., Kerridge, B., & Buchanan, S. M. (2009). Digital soil-class mapping from proximal and remotely sensed data at the field level. *Agronomy Journal*, *101*, 841–853.
- Van Groenigen, J. W., & Stein, A. (1998). Constrained optimization of spatial sampling using continuous simulated annealing. *Journal of Environmental Quality*, *27*, 1078–1086.
- Vina, A., Gitelson, A. A., Rundquist, D. C., Keydan, G., Leavitt, B., & Schepers, J. (2004). Monitoring maize (*Zea mays* L.) phenology with remote sensing. *Agronomy Journal*, *96*, 1139–1147.
- Viscarra Rossel, R., Walvoort, D., McBratney, A., Janik, L., & Skjemstad, J. (2006). Visible, near infrared, mid infrared or combined diffuse reflectance spectroscopy for simultaneous assessment of various soil properties. *Geoderma*, *131*, 59–75.
- Wald, L., Ranchin, T., & Mangolini, M. (1997). Fusion of satellite images of different spatial resolutions: assessing the quality of resulting images. *Photogrammetric Engineering & Remote Sensing*, *63*, 691–699.
- Welch, B. L. (1947). The generalization of student's' problem when several different population variances are involved. *Biometrika*, *34*, 28–35.
- Wheeler, D. C., & Páez, A. (2009). Geographically weighted regression. In M. M. Fischer & A. Getis (Eds.), *Handbook of applied spatial analysis. Software tools, methods and applications* (pp. 461–486). Berlin: Springer.